# Dual-stage 3D network super-resolution for volumetric fluorescence microscopy far beyond throughput limit

Hao Zhang[1+], Chunyu Fang[1+], Yuxuan Zhao[1+], Guo Li[1], Yi Li[4], Meng Zhang[2,3], Yusha Li[2,3], Peng Wan[2,3], Tingting Yu[2,3], Yuhui Zhang[2,3], Dan Zhu[2,3], Shangbang Gao[4], Peng Fei[1,2*]

[1] *School of Optical and Electronic Information, Huazhong University of Science and Technology, Wuhan, 430074, China.*

[2] *Wuhan National Laboratory for Optoelectronics, Huazhong University of Science and Technology, Wuhan, 430074, China.*

[3] *Britton Chance center for Biomedical Photonics, Wuhan National Laboratory for Optoelectronics, Huazhong University of Science and Technology, Wuhan 430074, China.*

[4] *College of Life Science and Technology, Huazhong University of Science and Technology, Wuhan, 430074, China.*

[+] *These authors contribute equally to this work*

[*] *Correspondence: feipeng@hust.edu.cn*

## Abstract

Though three-dimensional fluorescence microscopy has been an essential tool for modern life science research, the fundamentally limited optical throughput prevents its further move towards faster, clearer and higher-throughput applications. We hereby report a dual-stage, mutual-feedback 3D super-resolution network approach that allows gradient deep learning of the microscopy degradation from high-resolution targets to low-resolution images, which might be decimated in conventional end-to-end network approaches. Simply using single blurred-and-pixelated 3D image as input, our trained network is able to infer a 3D output with notably higher resolution as well as improved contrast. It thus can push the throughput limit of current 3D fluorescence microscopy from three striking aspects as: notably reducing the acquisition time for accurate mapping of large organs, breaking the diffraction limit for imaging subcellular events with faster, lower-toxicity measurement, and significantly improving temporal resolution for capturing instantaneous biological process. We demonstrate the success of this approach by imaging vessels/neurons in mouse brain at single-cell resolution and 10 minutes per whole brain throughput. We also image microtubules in single *U2OS* cell beyond the diffraction limit based on singe 3D acquisition at 2 Hz volume rate, and map neuronal activities of freely-moving *C. elegans* across 3400 × 800 × 60 μm field-of-view at single-cell resolution and 30 Hz volume rate.

## Introduction

A recurring trend in biology is the attempt to extract ever more spatial information from three-dimensional biological specimens in an ever short time. Many millisecond- dynamic cellular processes, such as functional activities occurring in live animals, requires high-speed capture of transient spatial patterns at high resolution. Massive cellular details distributed across very

large three-dimensional tissues also need to be obtained within an affordable time. These increasing quests are posing substantial challenge to current 3D light microscopy[1-3]. Traditional 3D imaging techniques, including Confocal and Two-photon excitation methods, can image samples in three dimensions at high spatial resolution. However, the relatively low acquisition rate together with epi-illumination mode is incapable of capturing 3D dynamics or large-scale imaging. The advent of light-sheet fluorescence microscopy has become a new technique-of-choice for volumetric imaging (LSFM) at relatively higher speed and lower phototoxicity, owing to the use of selective illumination at vicinity of focal plane and camera-based fast acquisition[4-10]. However, the optical information these imaging techniques could provide in a certain time, also known as optical throughput, remains unsatisfactory. For example, in each plane acquired by single snapshot, these microscopes are still incapable of either offering subcellular lateral resolution across large field of view of multicellular tissues, or breaking the diffraction limit for resolving organelles in single cell. On the other hand, these methods need to record many planes to comprise a 3D image with high-axial resolution, for which, however, the transient temporal profiles are decimated due to extended acquisition time. To improve the temporal resolution for capturing highly dynamic process, such as behaving model organisms, light field microscopy (LFM) particularly permits the retrieval of transient 3D signal distribution through post-processing of 4D light field recorded by single camera snapshot, but inevitably shows compromised spatial resolution and presence of reconstruction artefacts. Along another direction, various spatial resolution enhancement techniques, such as straightforward mechanical stitching[11-13], Fourier ptychographic microscopy[14,15], structured illumination microscopy (SIM)[16,17], single molecular localization microscopy[18-20], have been developed in past decade and greatly revolutionized the life science research. They provide a computational means of reconstructing a wide field-of-view (FOV), high-resolution (HR) 3D image or surpassing the diffraction limit based on a number of low-resolution (diffraction-limited) 3D images that have certain correlations in the space, frequency, or spectrum domain. However, these techniques apparently require increased acquisition time and complex computation procedure. Hence, despite either capturing 3D dynamics faster by one snapshot or achieving higher resolution by computing multiple image stacks, the optical throughput of these microscopy methods remains fundamentally limited and has so far prevented more widespread applications.

Unlike abovementioned multi-frame super-resolution techniques, single-image based super-resolution (SISR) methods can improve the resolution without necessarily increasing the imaging time, thereby increasing the imaging throughput. However, these methods suffer from either poor enhancement effect[21-23], or restriction of the signal characteristics[24,25]. Neural network-based super-resolution approaches have recently provided a paradigm shift in light microscopy[26-31], directly improving the spatial resolution for single input image by the inference of neural network that has been trained by label data in advance. Despite its advancement in stronger SISR capability combined with high reconstruction speed, the lack of super-resolution in three dimensions yet prevents its application to capture cellular events in 3D tissues at desired high throughput. Though CARE[28] uses U-net to increase the axial resolution of 3D microscopy image, it remains processing a 3D stack slice by slice in a 2D way. Furthermore, the quest on ever better super-resolution effect also intrinsically drive current network-based super-resolution methods towards newer structure and logic for applications now requiring

increasingly higher spatiotemporal performance.

Here we propose a novel imaging strategy based on dual-stage-processed neural network processing of 3D image data, termed DSP-Net, that can efficiently recover a fluorescence image stack with ~4-fold super resolution in three dimensions and tens of times higher signal-to-noise ratio. Our DSP-Net directly operates 3D image volumes rather than process them slice by slice. Also unlike traditional end-to-end network architecture, DSP-Net contains two mutual-feedback structures to perform de-blurring and de-pixelization trainings separately, fundamentally inverting the process in which the microscope transform a high-resolution target into a blurred and digitalized image. Through constructing such hierarchical training data with enriched distribution of frequency spectrum, this two-stage approach allows gradual deep learning of the transformation from low-frequency to high-frequency information which might be decimated in conventional super-resolution network architecture, resulting in stronger super-resolution capability. Once the network being properly trained, it could directly deduce super-resolved 3D image from recorded low-resolution image, showing ultra-high throughput suited for large-scale image reconstruction or time-lapsed video processing. To demonstrate the ability of DSP-Net combined with various imaging methods, such as Confocal, LSFM, N-SIM, to push the throughput limits of 3D fluorescence microscopy, we image neurons activities of freely-moving *C. elegans* across a 3400 μm × 800 μm × 60 μm ultra-large FOV at single-neuron resolution, extracting the spatiotemporal patterns of neuronal calcium signaling and tracking correlated worm activity at volume rate of 30 Hz, notably faster than conventional Bessel LSFM. We also demonstrate 3D imaging of organelles in single *U2OS* cell at 2 Hz volume rate as well as sub-100 nm spatial resolution that is unmet by conventional N-SIM, and 3D anatomical mapping of neurons/vessels in whole mouse brain at single-cell resolution as well as ultra-high throughput of 10 minutes per brain, which is at least 2-orders higher than that from either conventional confocal or LSFM.

## Result

### DSP-Net for 3D super resolution

An end-to-end super-resolution neural network is able to fit complex mapping functions only when sufficient parameters are provided. Practically, owing to the highly nonlinear relationship in the ill-posed SISR problem, it is often difficult to directly map the single low-resolution (LR) input to its high-resolution (HR) target perfectly as expected, especially when they have significant quality gap, or in another word, a notable quality improvement is desired. We mitigate this network limitation by logically solving the SISR problem by two steps as: extracting rich details from the badly decimated LR input and enhancing the true signals while suppressing noises and the background. These two steps also fundamentally correspond to the recovery of digital signal aliasing by camera pixelization, and the restoration of optical blurring by the objective with limited numerical aperture (NA). Accordingly, we create a resolver and an interpolator modules in our DSP-Net, with each containing independent training target corresponding to the solution of 2 sub-issues. Complying with standard deep learning strategy, our DSP-Net comprises a training and an inference phases (Fig. 1a, b). At the training phase, the neural network establishes its super-resolution ability from scratch by learning from a bunch of examples (i.e., the training dataset). HR isotropic 3D images, regarded as ground truth, were acquired using scanned Bessel light microscopes with high-magnification/ high-NA objectives,

or in the case for breaking diffraction limit, by Bessel light-sheet microscope combined with 3D SRRF techniques[32]. We then applied an image degradation model(Supplementary Note 1), including optical blurring, down-sampling and noise addition, to the ground truths to generate synthetic LR images, which was corresponded to our LR measurement under low-magnification/low-NA setups (Fig.1a, step1). Meanwhile, a directly down-scaled version of the ground truths, termed mid-resolution (MR) data, was also generated as aliased results to bridge the two-stage training (Fig.1a, step2). With these synthetic training pairs prepared, the LR images were first fed to the super-resolver for clearing the noises and the backgrounds while retaining the potential high frequency structures. (Fig.1a, step3). The mean square error (MSE) between the MR and the output of the super-resolver, termed MR', was defined as the resolving loss, to evaluate the output quality of the super-resolver (Fig.1a, step4). The MR' outputs were then sent the interpolator to be up-sampled (4 times in each dimension) into the super-resolution results (SR), with their high-frequency features being extracted and further enhanced (Fig.1a, step5). We further defined the MSE between the HR ground truths and the SR outputs as the interpolating loss (Fig.1a, step6). By iteratively minimizing the two loss functions using a gradient descent approach, the parameters of both sub-nets could be optimized gradually, empowering the whole DSP-Net with ability to recover SR outputs from LR inputs with quality very close to HR ground truths. Once the training of DSP-Net converged to an optimal status, blurred, noised and pixelated 3D images captured by low-magnification/low NA (or diffraction-limited) setups could be input to the trained DSP-Net, to be recovered into a higher-resolution, higher-contrast, de-pixelated outputs directly without iterative computation required (Fig. 1a, step7). By substantially increasing the spatial resolution without repetitive imaging/stitching, DSP-Net greatly improves the optical throughput, known as the spatial information can be obtained per unit time, of 3D fluorescence microscopy, which is originally limited by the system optics, regardless of its employed magnification factor or numerical aperture (NA). Compared to the existing one-stop networks[33-36], this DSP-Net leads to a more efficient optimization, resulting in a lower training time consumption and a better restoration quality, which was shown in the following experiment results.

We first demonstrated the DSP-Net based light-sheet imaging of labeled blood vessels in mouse brain. The raw 3D image stack of vessels, acquired by a Bessel light-sheet microscope using 3.2×/0.2 detection combined with ~3-μm thickness plane illumination, encompassed 4.2 billion isotropic voxels (2 μm) across 4.16 mm × 4.16 mm × 4 mm large FOV (Fig. 2b, left). Vignette high-resolution view of the vessel shows inadequate resolving power due to low NA and relatively large voxel (Fig. 2b, LR), as compared to the HR reference acquired by 12.6×/0.5 detection combined with ~1-μm plane illumination (0.5-μm voxel, Fig. 2b, HR). DSP-Net recovered a 3D image with resolution close to that of the HR reference while kept high reconstruction fidelity with minimal artefacts. We further compared our DSP-Net results with those by a state-of-art single-stage network RDN[34,35] (Fig.1 d), showing higher spatial resolution (Fig. 1 e) as well as better signal-to-background ratio (SBR).

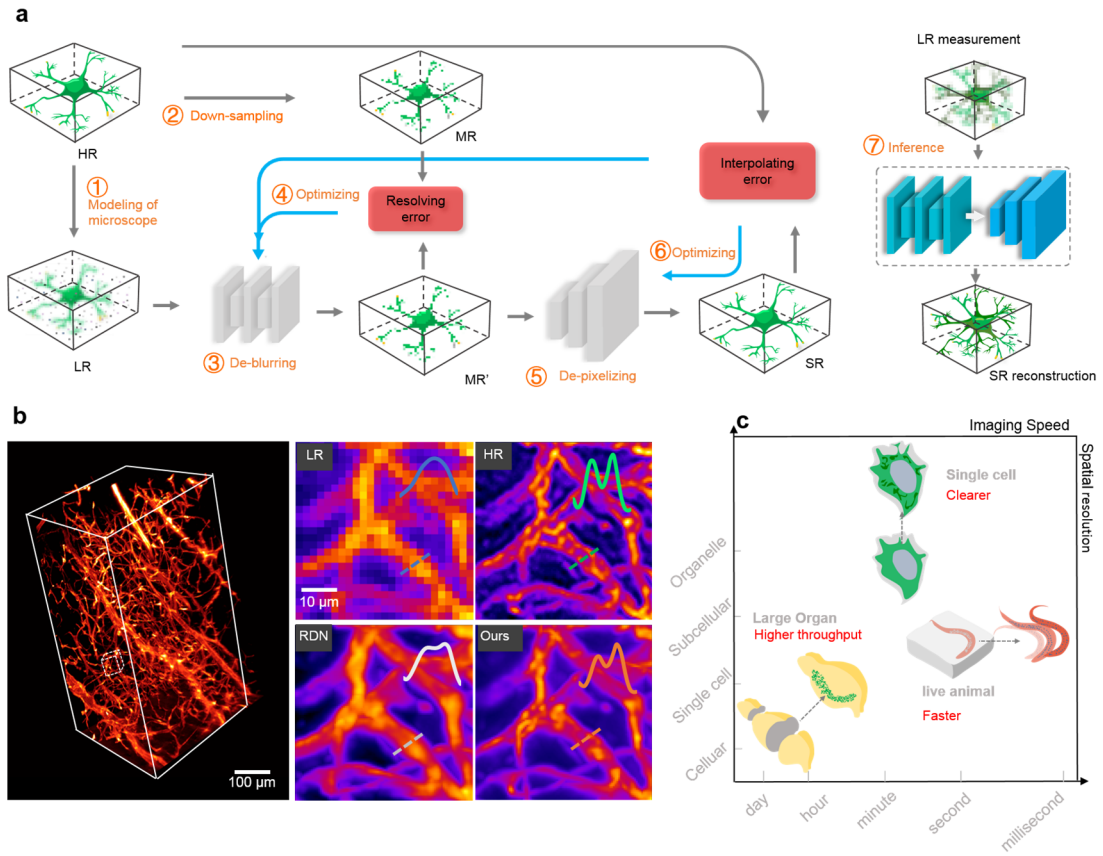


**Fig. 1 | DSP-Net**. **a**, pipeline of training the DSP-Net and the inference phase. HR image volumes are acquired with densely scanning light sheet under high magnification objective. Through a degrading model that imitates the transfer function of the imaging system, LR volumes are generated (step 1). The corresponding MR volumes are directly down-sampled from the HRs (step 2). The first stage of DSP-Net, i.e. the resolver takes the LR as the input, suppressing its noises and the background (step3). The output of the resolver, named MR', is the intermediate result for computing the resolving error with the MR. The parameters of the resolver get optimized by minimizing the resolving error (step 4). The MR' is further input to the interpolator to reconstruct the high frequency structures (step 5). The MSE between the HR and the output of the interpolator is defined as the interpolating error. Both the interpolator and the resolver are responsible for the interpolating loss, thus minimizing it would result in the optimization of both sub-nets (step 4, 6). After well trained, a LR measurement is obtained with a sparsely scanning light sheet under a low magnification objective, and used as the input to the DSP-Net. The network makes an end-to-end super resolution by directly output the enhanced image volume. The training process requires high computational power devices such as GPU, while the inference can be conducted on any common computers. **b,** 3-D rendering of the DSP-Net results of the mouse brain vessel LSFM images. Shown are X-Y cross sections of the input LR, the HR ground truth, the RDN results and the DSP-Net result, with the resolution plot of the line-cut. **c**, DSP-Net enables faster imaging speed, higher resolution and higher throughput in traditional microscopy.

**3D isotropic imaging of single neurons in whole mouse brain at minutes time-scale**

We imaged GFP-tagged neurons in whole mouse brain (Thy1-GFP-M) at ultra-high throughput. The cleared whole brain has a large size of ~10 mm × 8 mm × 5 mm with highly heterogeneous fine neuronal structures distributed in hundreds of brain regions. Even with the use of our self-built light-sheet microscope that has relatively high acquisition speed, single-cell-resolution volumetric mapping of whole brain remains highly challenging, owing to the limited system throughput, and thereby requires long-lasting tile imaging, e.g., nearly 200 tiles in tens of hours, under a high-magnification setup, e.g., 12.6× detection with 1-μm plane illumination.

In our DSP-Net Bessel light-sheet implementation (Fig. 2a), we first chose high-resolution, high-SBR Bessel images of a few neurons (abovementioned 12.6× setup, 500 ms exposure) in isocortex and cerebellum regions to construct training dataset for DSP-Net, and then used the trained network to restore low-resolution, low-SBR images of various types of neurons across the whole brain (abovementioned 3.2× setup, 50 ms exposure). In Fig. 2b, we showed the DSP-Net recovered 3D neurons from cortex (b2, middle column), striatum (b3, middle column) and cerebellum (b4, middle column) regions of reconstructed whole brain (b1), and compared the results with raw 3.2× inputs (left columns) as well as HR reference images by the same 12.6× setup used for the acquisition of training data (right columns). We notice that the recovered images by DSP-Net show obviously sharper details of neuron fibers, as compared to the ambiguous LR inputs, providing near-isotropic 3D resolution as high as that of HR reference (plots in Fig. 2b). Therefore, DSP-Net enabled Bessel light-sheet microscopy herein shows its strong capability for rapid whole-brain imaging, typically in a few minutes under 3.2× acquisition, at single-neuron resolution, which is close to those by 12.6× HR setup. Its achieved throughput could be over 2-orders higher than conventional Bessel light-sheet (Fig. 2c). Furthermore, it is shown that the extra robustness of neural network also allows our DSP-Net to be quickly trained by merely a small amount of HR neuron data, before it can recover various types of neurons in whole brain. As a result of high-throughput, high-resolution mapping of whole brain, the segmentation and tracing of long-distance neurons, as well as image-based quantitative analysis could be performed at system level. As a demonstration, we segmented a pyramidal neuron at cortex region. Compared to the raw 3.2× image, DSP-Net obviously visualized more nerve fibers, thus enabling neuronal trajectory with more abundant details of connectivity presented in three dimensions (Fig. 2d).

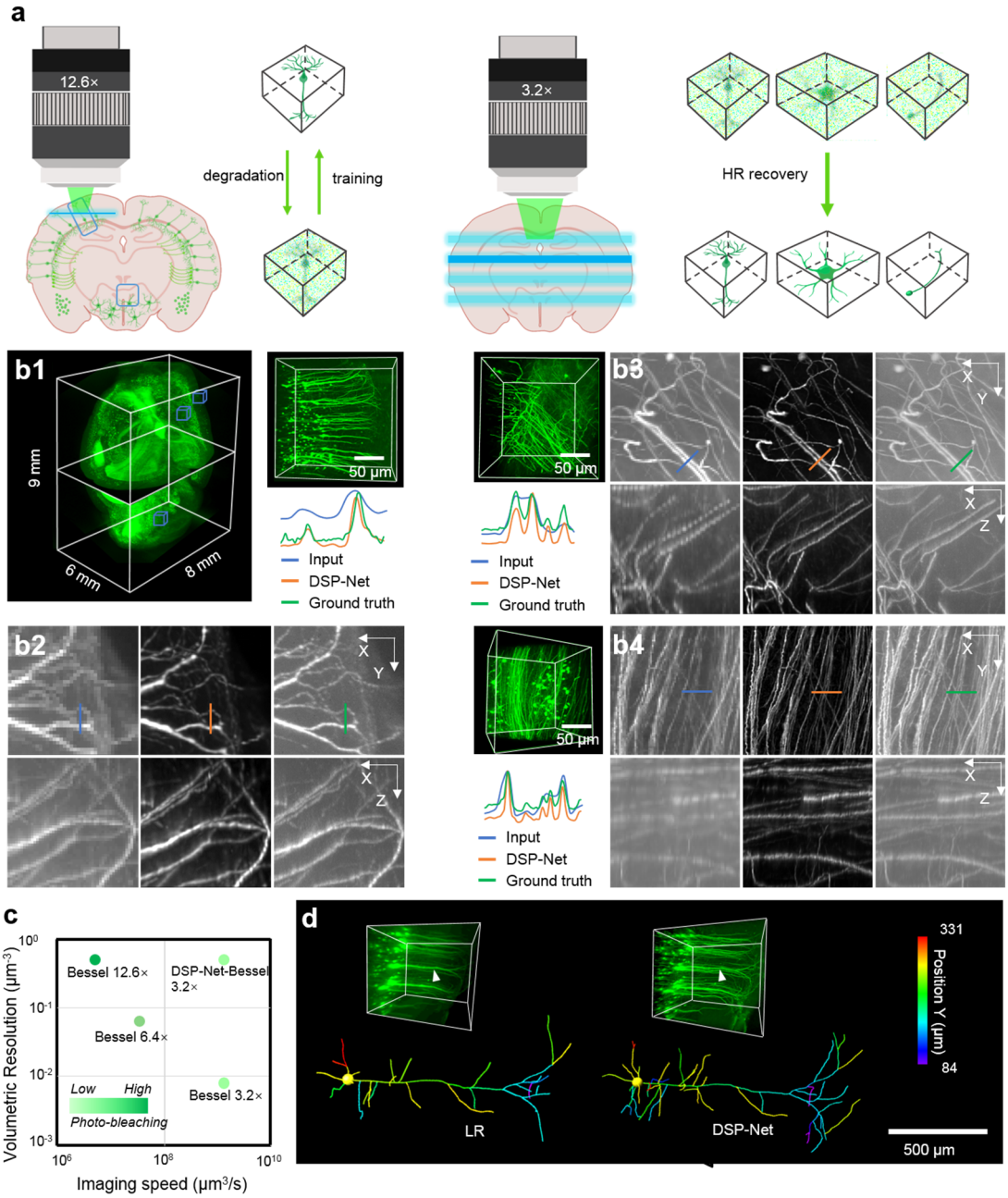


**Fig. 2 | DSP-Net on whole mouse brain.** For Thy1-GFP-M whole mouse brain, DSP-Net increases resolution ×4 in each dimension, which offers much higher throughput in some applications like neuron tracing. **a**, Whole work flow includes data acquisition with 3.2× and 12.6×, HR degradation for obtaining training pair, network training and high-resolution image output. **b**, Recover three ROIs from different encephalic regions. XY and XZ planes show comparison of details among input LR, network output and ground truth HR from cortex **b2**, striatum **b3** and cerebellum **b4**. Profile of linecuts quantify the resolution enhancement. **c,** Effect of DSP-Net on neuron tracing in a small region from cortex. Based on both LR data and network output, the same single neuron is traced from apical dendrites to cell body with Imaris. **d**, Throughput comparison of different modes, include 3.2×, 6.4×, 12.6×and DSP-Net on 3.2×.

**Rapid 3D super-resolution imaging of single cell with low photo-toxicity**

A common problem in super-resolution fluorescence microscopy in sub-cellular level is the photon budget for reconstructing super-resolution images. We demonstrate the ability of DSP-Net by imaging Alexa Fluor 488-labelled microtubules in single *U2OS* cell beyond the diffraction limit, with improved acquisition rate as well as reduced photon budget. We first obtained sub-diffraction-limit 3D image of microtubules based on super-resolution radial fluctuations (SRRF)[32] computation of thirty diffraction-limited image stacks consecutively acquired by our Bessel light-sheet microscope (Method). Due to the noticeable photo-bleaching by repetitive fluorescence emission, the last one of the 30 image stacks obviously shows lowest SNR as well as diffraction-limited resolution, equivalent to the image stack acquired by a lower-intensity laser illumination. Then we used the 3D-SRRF image and its corresponding LR images to construct training dataset for DSP-Net, and applied the trained network to the super-resolution of the $30^{th}$ measurement with lowest quality (Fig.3 a). We demonstrate that for low-resolution, low-SNR input data obtained by diffraction-limited optics and low-dose excitation (few photon emission), the DSP-Net enables notable improvement in both 3D resolution and SNR (Fig. 3c). The network was also proven to be highly robust, capable of recovering high-fidelity super-resolution image stack from either $1^{st}$ or $30^{th}$ stack of the 30 measurements (Fig. 3c). The line profiles of the resolved microtubules by low-SNR, high SNR inputs, their corresponding DSP-Net outputs, and SRRF result, were plotted in Fig. 3d, to compare the achieved resolution by each method. The quality of DSP-Net recovery is similar with SRRF results (Fig. 3d) while the network consumes less than 0.05% photons to reconstruct the super-resolution image (Fig. 3f). Therefore, DSP-Net combined with light-sheet microscopy permits very low-toxic, low-beaching super-resolution 3D imaging with minimal-intensity excitation, indicating its strong potential for sustained live cell imaging . Considering the SISR capability of DSP-Net, it exhibits beyond-diffraction-limit resolution (~100 nm) similar with SRRF result while keeps a temporal resolution as high as standard Bessel sheet imaging, at a rate of around 2 volume $s^{-1}$(Fig. 3g).

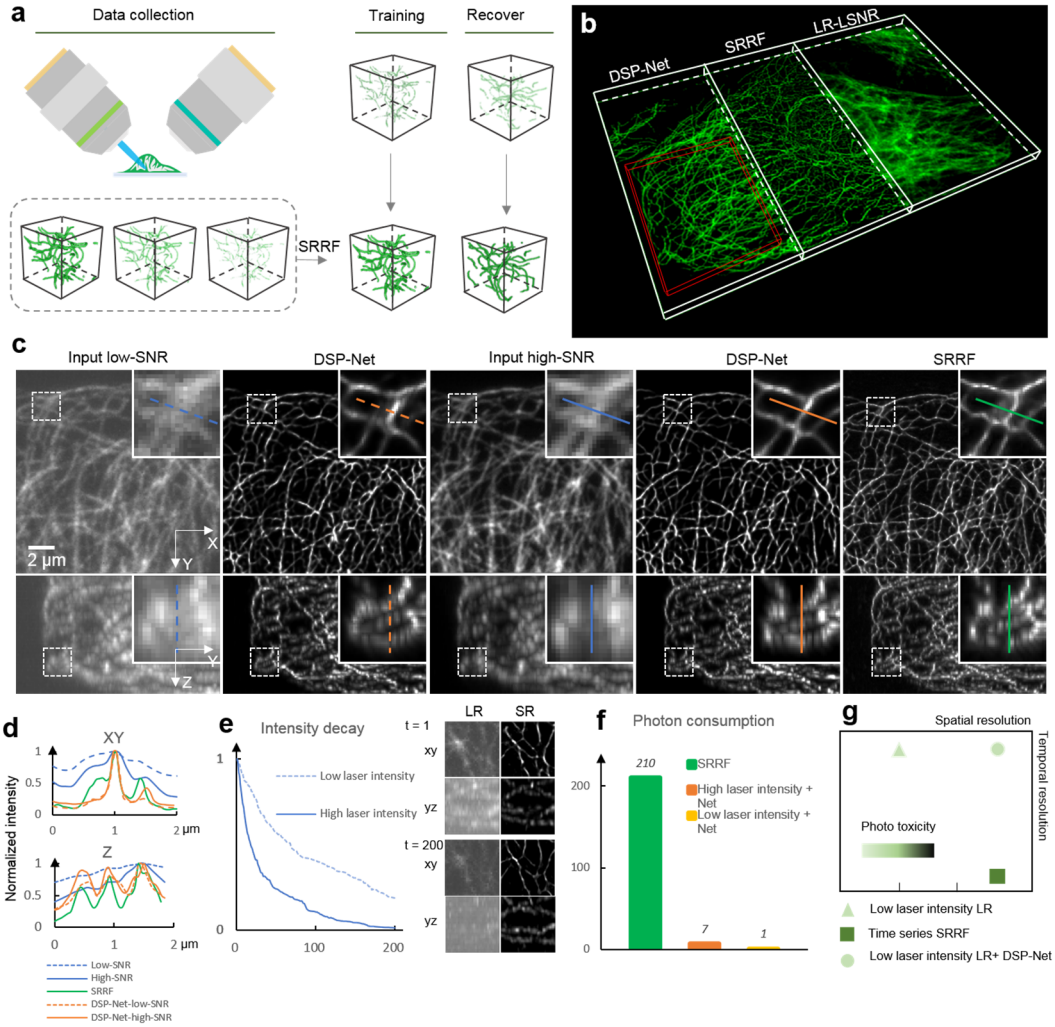


**Fig. 3 | Resolving sub-diffraction structure at low photon budget. a**, Schematic of training data collection and network construction. **b**, Volume rendering of antibody-labeled microtubules in fixed U2OS. **c**, Magnified images in xy and yz plans from the red box region in b. Shown are low resolution low SNR input data, corresponding network reconstruction results, low resolution high SNR input data, and corresponding network reconstruction results, and super-resolution radial fluctuations reconstruction results. **d,** Line plots show image intensities along the lines. **e**, Comparison of photo-bleaching rates of microtubules over 200 acquired volumes with different laser intensity. And reconstructed results in xy and yz plane for the first and 200$^{th}$ volumes. **f**, Comparison of the photon consumption of different method for reconstructing super resolution images. **g,** The trade − off between temporal resolution, spatial resolution and photo-toxicity. DSP-Net loosens this constrains.

## Cross-mode 3D super-resolution by DSP-Net

We directly use the DSP-Nets trained by Bessel light-sheet images of brain neurons, or SRRF Bessel light-sheet images of microtubules in cells, to restore the low-resolution images of the neurons by confocal microscope, or diffraction-limited wide-field image of the microtubules

by SIM microscope, respectively. As shown in Fig. 4a, 3D images stack of a 100-μm thick mouse brain slice was captured by a confocal microscope (Nikon Ni-E, CFI LWD 16×/0.8 W objective). The down-sampled version (4 × 4 × 4 times in three dimensions) of the confocal stack, considered as the LR inputs (Fig. 4b, LR), was then sent to the abovementioned DSP-Net trained with Bessel light-sheet data, for cross-mode (CM) super-resolution inference. The result, termed as CM-DSP-Net in Fig 4b, was further compared with the recovered result by another DSP-Net normally trained with confocal data (DSP-Net), as well as the original HR 16× confocal measurement (Fig. 4b, HR). For super-resolution 3D imaging of microtubules in an *U2OS* cell (Fig. 4e), the LR input was a diffraction-limited 3D wide-field image obtained by simply averaging the fifteen SIM exposures at each z-plane ( Nikon N-SIM,CFI Apo TIRF 100x/1.49 oil, Fig. 4f, LR). The abovementioned DSP-Net trained using Bessel light-sheet data was then applied to this wide-field image to recover 3D microtubules beyond diffraction limit (Fig. 4f, CM-DSP-Net). The result was finally compared with super-resolution image obtained by 3D-SIM reconstruction using the 15 patterned exposures (Fig. 4f, 3D-SIM). For both case, these cross-mode DSP-Net could provide extraordinary enhancement to the heterogeneous inputs. By qualitatively analyzing the reconstruction quality, CM-DSP-Net results show spatial resolutions similar with those by regular DSP-Net. At the same time, the high RSP and RSE values also indicate the sufficient accuracy of the CM-DSP-Net recovery.

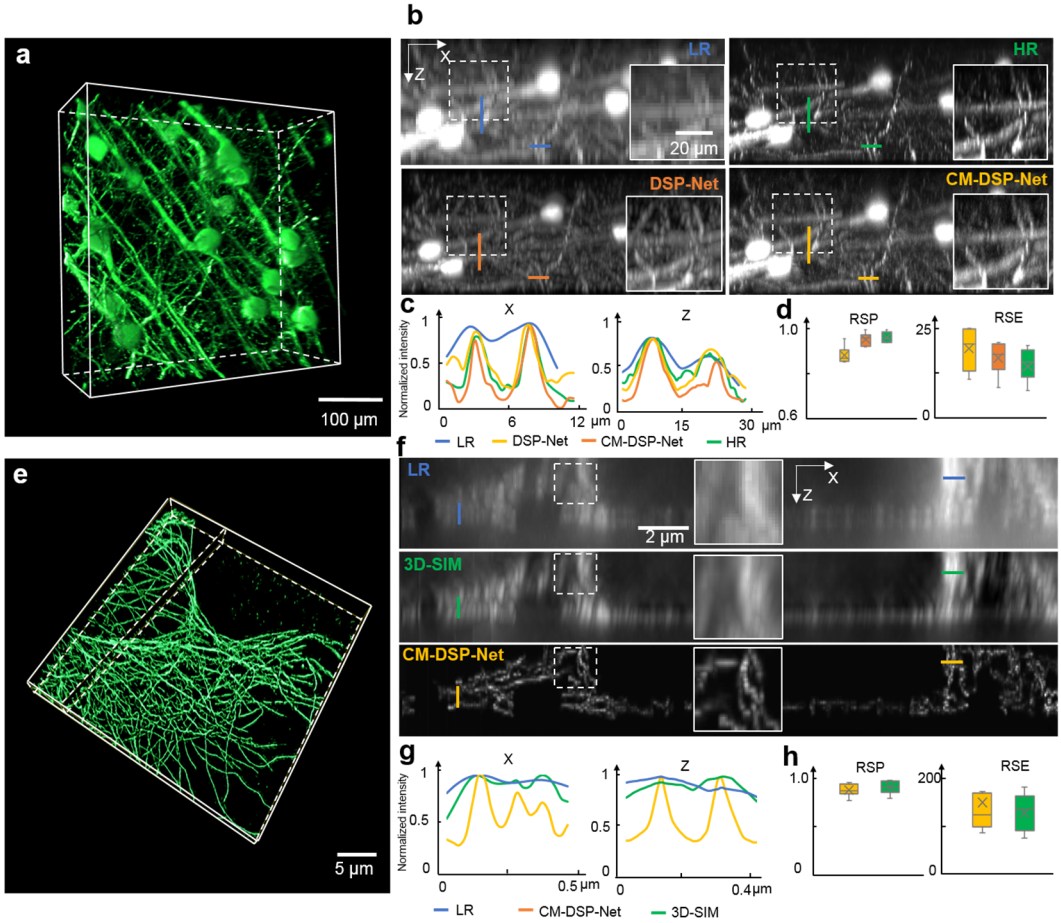


**Fig. 4 | Cross-mode imaging by DSP-Net. a,** 3D images stack of a 100-μm thick mouse brain slice reconstructed by the CM-DSP-Net. **b**, XZ projections of the 4× confocal image, 16× confocal image, reconstruction of DSP-Net and CM-DSP-Net, respectively . **c,** Plots of the normalized intensity of the

linecuts in the lateral (X) and axial (Z) planes in **b**. **d,** RSP and RSE of the DSP-Net outputs, CM-DSP-Net outputs and the HRs with respect to the LR input images. **e,** CM-DSP-Net reconstruction of the diffraction limited wide-field images of U2OS cells labeled with microtubes. **f,** XZ projections of the input, 3D-SIM reconstruction and the CM-DSP-Net reconstruction, respectively. **g,** Plots of the normalized intensity of the linecuts in the lateral (X) and axial (Z) planes in **f**. **h,** RSP and RSE of the CM-DSP-Net outputs and the 3d-SIM outputs with respect to the LR input images.

**Cross-sample 3D super-resolution by DSP-Net.**

In addition to cross-mode capability, we further demonstrate that the DSP-Net also enables cross-sample (CS) super-resolution imaging of brain vessels by a brain neuron-trained network at single cell resolution, and endoplasmic reticulum by a microtubules-trained network beyond the diffraction limit. For both cases, our network shows intrinsically remarkable improvements for new types of signals (Fig. 5a,b, d, e). Furthermore, the quantitative analyses on achieved resolution and reconstruction errors both verify the reliable cross-sample super-resolution recovery by DSP-Net. It's noted that the robust cross-mode, cross-sample capabilities found in our 3D DSP-Net were also consistent with previous findings from 2D network super-resolution[27].

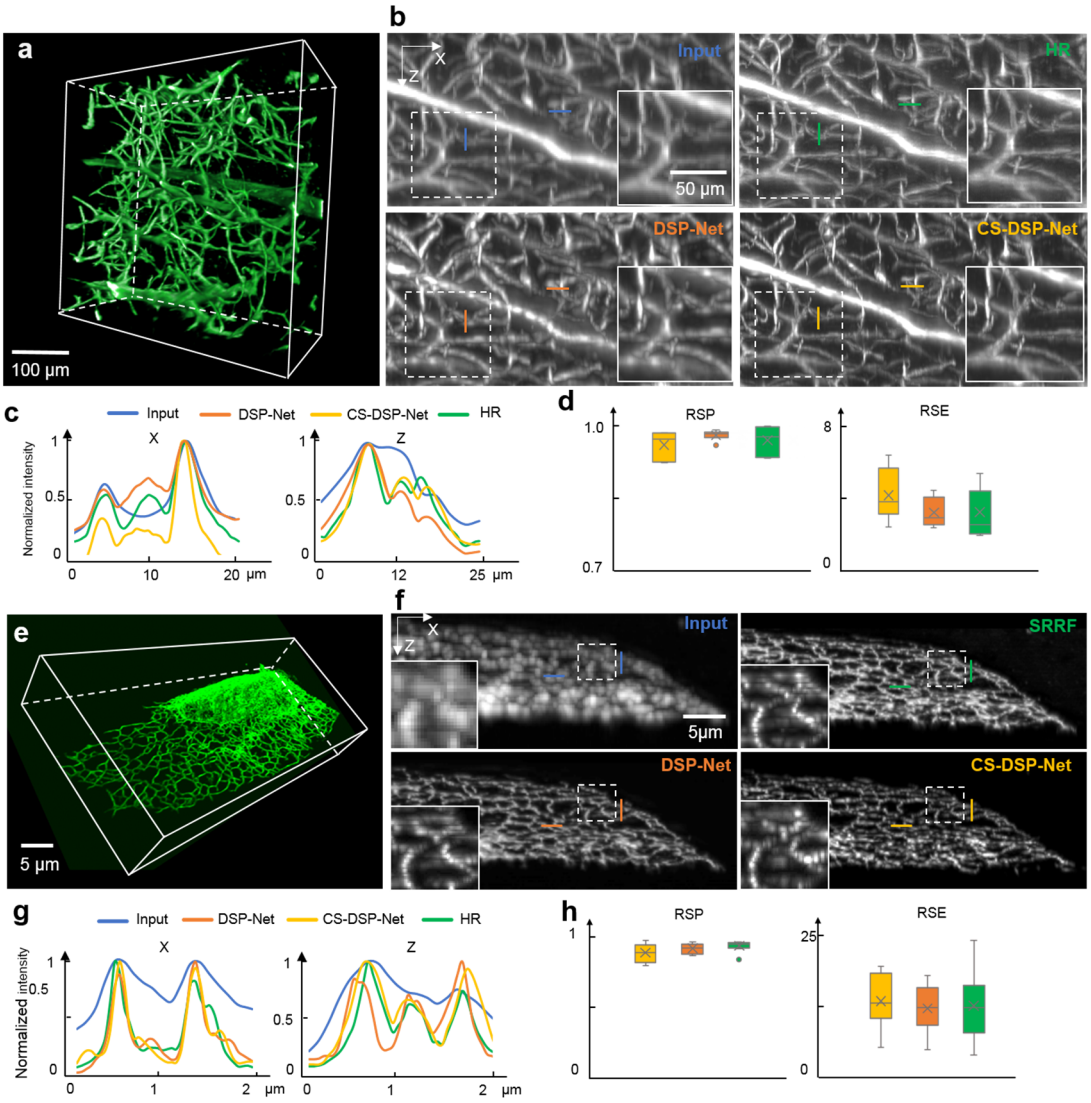


**Fig. 5 | Cross-sample imaging by DSP-NET.** **a,** DSP-NET shows cross-sample imaging capability on Alexa647 labelled mouse brain vessels. **b**, XZ projections of the LR input, HR, reconstruction of DSP-Net and CS-DSP-Net, respectively . **c,** Plots of the normalized intensity of the linecuts in the lateral (X) and axial (Z) planes in **b**. **d,** RSP and RSE of the DSP-Net outputs, CS-DSP-Net outputs and the HRs with respect to the LR input images. **e,** DSP-NET shows cross-sample imaging capability on U2OS cells labeled with microtubes. **f,** XZ projections of the LR input, SRRF result, DSP-Net and CS-DSP-Net output, respectively . **g,** Plots of the normalized intensity of the linecuts in the lateral (X) and axial (Z) planes in **f**. **h,** RSP and RSE of the DSP-Net outputs, CS-DSP-Net outputs and the HRs with respect to the LR input images.


## Funding

National Key R&D program of China (2017YFA0700500), the National Natural Science Foundation of China (21874052, 61860206009 and 31671052), the Innovation Fund of WNLO, and Junior Thousand Talents Program of China.

# References


1 Pawley, J. B. Handbook of Biological Confocal Microscopy. *Journal of Biomedical Optics* **25**, 029902 (1995).

2 Denk, W., ., Strickler, J. H. & Webb, W. W. Two-photon laser scanning fluorescence microscopy. *Science* **248**, 73-76 (1990).

3 Jan, H., Jim, S., Filippo, D. B., Joachim, W. & Stelzer, E. H. K. Optical sectioning deep inside live embryos by selective plane illumination microscopy. *Science* **305**, 1007-1009 (2004).

4 Keller, P. J., Schmidt, A. D., Wittbrodt, J. & Stelzer, E. H. K. Reconstruction of Zebrafish Early Embryonic Development by Scanned Light Sheet Microscopy. *Science* **322**, 1065-1069 (2008).

5 Ahrens, M. B., Orger, M. B., Robson, D. N., Li, J. M. & Keller, P. J. Whole-brain functional imaging at cellular resolution using light-sheet microscopy. *Nature Methods* **10**, 413 (2013).

6 Verveer, P. J. *et al.* High-resolution three-dimensional imaging of large specimens with light sheet-based microscopy. *Nature Methods* **4**, 311-313 (2007).

7 Huisken, J., Swoger, J., Bene, F. D. & Wittbrodt, J. Optical Sectioning Deep inside Live Embryos by Selective Plane Illumination Microscopy. *Science* **305**, 1007-1009 (2004).

8 Ritter, J. G., Veith, R., Veenendaal, A., Siebrasse, J. P. & Kubitscheck, U. Light Sheet Microscopy for Single Molecule Tracking in Living Tissue. *Plos One* **5**, e11639 (2010).

9 Tomer, R., Khairy, K., Amat, F. & Keller, P. J. Quantitative high-speed imaging of entire developing embryos with simultaneous multiview light-sheet microscopy. *Nature Methods* **9**, 755 (2012).

10 Keller, P. J. *et al.* Fast, high-contrast imaging of animal development with scanned light sheet-based structured-illumination microscopy. *Nature Methods* **7**, 637 (2010).

11 Mikula, S., Trotts, I., Stone, J. M. & Jones, E. G. Internet-enabled high-resolution brain mapping and virtual microscopy. *Neuroimage* **35**, 9-15 (2007).

12 Lichtman, J. W. & Winfried, D. The big and the small: challenges of imaging the brain's circuits. *Science* **334**, 618-623 (2011).

13 Murakami, T. C. *et al.* A three-dimensional single-cell-resolution whole-brain atlas using CUBIC-X expansion microscopy and tissue clearing. *Nature Neuroscience* **21** (2018).

14 G, Z., R, H. & C, Y. Wide-field, high-resolution Fourier ptychographic microscopy. *Nature Photonics* **7**, 739-745 (2013).

15 Ou, X., Zheng, G. & Yang, C. Embedded pupil function recovery for Fourier ptychographic microscopy. *Optics Express* **22**, 4960-4972 (2014).

16 Gustafsson, M. G. L. Surpassing the lateral resolution limit by a factor of two using structured illumination microscopy. *Journal of Microscopy* **198**, 82-87 (2010).

17 Gustafsson, M. G. L. Nonlinear structured-illumination microscopy: wide-field fluorescence imaging with theoretically unlimited resolution. *Proceedings of the National Academy of Sciences of the United States of America* **102**, 13081-13086 (2005).

18 Hell, S. W. & Wichmann, J., . Breaking the diffraction resolution limit by stimulated emission: stimulated-emission-depletion fluorescence microscopy. *Optics Letters* **19**, 780-782 (1994).

19 Rust, M. J., Bates, M. & Zhuang, X. Stochastic optical reconstruction microscopy (STORM) provides sub-diffraction-limit image resolution. *Nature Methods* **3**, 793 (2006).

20 Eric, B. *et al.* Imaging intracellular fluorescent proteins at nanometer resolution. *Science* **313**, 1642-1645 (2006).

21 Freeman, W. T., Jones, T. R. & Pasztor, E. C. Example-based super-resolution. *Computer Graphics & Applications IEEE* **22**, 56-65 (2002).

22 Duchon, C. E. Lanczos Filtering in One and Two Dimensions. *J.appl.meteor* **18**, 1016-1022 (1979).

23 Li, X., . & Orchard, M. T. New edge-directed interpolation. *IEEE Trans Image Process* **10**, 1521-1527 (2001).

24 Kwang In, K. & Younghee, K. Single-image super-resolution using sparse regression and natural image prior. *IEEE Transactions on Pattern Analysis & Machine Intelligence* **32**, 1127 (2010).

25 Weisheng, D., Lei, Z., Guangming, S. & Xiaolin, W. Image deblurring and super-resolution by adaptive sparse domain selection and adaptive regularization. *IEEE Transactions on Image Processing* **20**, 1838-1857 (2011).

26 Rivenson, Y. *et al.* Deep learning microscopy. *Optica* **4**, 1437-1443, doi:10.1364/OPTICA.4.001437 (2017).

27 Wang, H. *et al.* Deep learning enables cross-modality super-resolution in fluorescence microscopy. *Nature Methods* **16**, 103-110, doi:10.1038/s41592-018-0239-0 (2019).

28 Weigert, M. *et al.* Content-aware image restoration: pushing the limits of fluorescence microscopy. *Nature Methods* **15**, 1090-1097, doi:10.1038/s41592-018-0216-7 (2018).

29 Zhang, H. *et al.* High-throughput, high-resolution deep learning microscopy based on registration-free generative adversarial network. *Biomedical Optics Express* **10**, 1044-1063, doi:10.1364/BOE.10.001044 (2019).

30 Ozcan, A. *et al.* Deep learning microscopy. *Optica* **4**, 1437- (2017).

31 Zhang, H. *et al.* High-throughput, high-resolution deep learning microscopy based on registration-free generative adversarial network. *Biomedical Optics Express*.

32 Gustafsson, N. *et al.* Fast live-cell conventional fluorophore nanoscopy with ImageJ through super-resolution radial fluctuations. *Nature Communications* **7**, 12471 (2016).

33 Haris, M., Shakhnarovich, G. & Ukita, N. Deep Back-Projection Networks For Super-Resolution. *arXiv e-prints* (2018). <https://ui.adsabs.harvard.edu/abs/2018arXiv180302735H>.

34 Zhang, Y., Tian, Y., Kong, Y., Zhong, B. & Fu, Y. Residual Dense Network for Image Restoration. *arXiv e-prints* (2018). <https://ui.adsabs.harvard.edu/abs/2018arXiv181210477Z>.

35 Zhang, Y., Tian, Y., Yu, K., Zhong, B. & Yun, F. Residual Dense Network for Image Super-Resolution. (2018).

36 Haris, M., Shakhnarovich, G. & Ukita, N. Deep Back-Projection Networks For Super-Resolution. (2018).